ELSEVIER

International Journal of Heat and Fluid Flow 21 (2000) 264–270

International Journal of HEAT AND FLUID FLOW

www.elsevier.com/locate/ijhff

Scrutinising flow field pattern around thick cambered trailing edges: experiments and computations

E. Coustols [a,*], G. Pailhas [a], P. Sauvage [b]

[a] *Department of Modelling in Aerodynamics and Energetics, ONERA/DMAE, 2 avenue Edouard Belin, 31 055 Toulouse cedex, France*
[b] *AEROSPATIALE A/SW/SF, 316 Route de Bayonne, 31 060 Toulouse cedex, France*

Received 21 September 1999; accepted 8 February 2000

Abstract

A detailed experimental study has been launched at ONERA/DMAE, aiming at the description of the flow pattern in the vicinity of thick cambered trailing edges. LDV and pressure measurements have provided a very detailed database, which has been considered, for validation of computational tools. Thus, several one- and two-equation turbulence models, implemented in the Reynolds-averaged Navier–Stokes (RANS) solver developed at ONERA, have been applied to the experimental configurations. Typical features are carefully discussed with emphasis set on both pressure distributions (prediction of correct rear loading) and near-wake surveys (capture of the topological vortex-type structure).

Keywords: Turbulence; Modelling; Cambered trailing edge; Wake

1. Introduction

Research has been conducted rather recently at ONERA, in the field of supercritical airfoils equipped with thick cambered trailing edges. For transonic applications, the aerodynamic performance of such airfoils, previously referred to as "Divergent Trailing Edge" (DTE) (Henne and Greg III, 1991), could be put forward mainly from computational tools. Indeed, when considering relatively high values of the lift coefficient, total drag reduction could be evident in spite of base drag increase, because of increased airfoil loading and subsequent wave drag decrease.

As the physical aspects induced by such non-conventional trailing edge geometries are identical, whatever flow regime is considered, a rather detailed experimental study has been undertaken at the hydrodynamic tunnel of ONERA. The aim is to scrutinise the flow field pattern downstream of an airfoil equipped with three non-zero-thickness trailing edges: (i) a reference trailing edge (RTE) having a base thickness of 0.5% airfoil chord length (c or C); (ii) two increased cambered trailing edges with the same trailing edge angle, but different incremental base thicknesses, either 0.2% c (CTE 1) or 0.5% c (CTE 2).

Apart from static pressure measurements, a two-dimensional laser doppler velocimetry (LDV) system, operating in the backward-scattering mode, has provided very detailed velocity measurements in the close vicinity of each trailing edge. Experiments have been conducted at turbulent conditions, for a free stream Reynolds number (based upon c) less than 1 million.

The hypothesised flow field pattern has been carefully characterised: a very complete database has been generated for several trailing edge shapes (Pailhas et al., 1998, Sauvage, 1998). This database is used for validating the computational tools that will be considered for future optimisation of specific wing design with non-zero thickness trailing edges. Consequently, a numerical approach has been conducted, aiming at testing the behaviour of different turbulence models under such aerodynamic and geometric conditions.

The Reynolds-averaged Navier–Stokes (RANS) solver, developed by ONERA (Vuillot et al., 1993, Couaillier, 1999), has been applied to the airfoil with the tested trailing edge geometries. Grid generation has led to a "C–H" type mesh topology, with specific refinement in the vicinity of the cambered trailing edges. Several one- and two-equation transport models have been considered.

Detailed comparisons between experiments and computations are discussed with a special emphasis being placed on pressure distributions, boundary layer and near-wake surveys in the trailing edge vicinity.

2. Experimental study

2.1. Water tunnel

Experiments have been carried out in the circulatory-type water tunnel of ONERA/DMAE (Pailhas et al., 1998). The horizontal test section is 0.5 m large, 0.3 m high and 3 m long; the lateral walls allow perfect optical access for LDV

* Corresponding author. Tel.: +33-5-62252815; fax: +33-5-62252583.
E-mail address: eric.coustols@onecert.fr (E. Coustols).

0142-727X/00/$ - see front matter
PII: S0142-727X(00)00008-4

measurements. The velocity variations at the test section entrance are lower than 1% of the mean velocity. The main parameters governing the flow are constantly controlled and adjusted by a microcomputer via an automaton.

2.2. Model

The reference model for the present investigation is an OAT15A airfoil having a maximum thickness ratio of 12.3% and 400 mm of c; the upper surface contour is constrained to be the same as the original OAT15A whereas the airfoil geometry is modified on the lower surface only.

The airfoil is manufactured in such a way that the rear part (last 19% and 15% c of the upper and lower sides, respectively) is removable, allowing to mount rather easily the different shapes of trailing edges to be tested. The three following two-dimensional trailing edges have been considered (Fig. 1):

The Reference Trailing Edge (RTE), having a base thickness of 0.5%C.

Two increased cambered trailing edges, CTE 1 and CTE 2, with the same trailing edge angle, but different incremental base thicknesses: 0.2%C and 0.5%C, respectively.

The geometry of these trailing edges results from a numerical optimisation performed at ONERA/DAAP using a compressible Euler method coupled with an integral boundary layer method, referred to as "ISES" (Drela and Giles, 1987).

The model, with the RTE, is fitted with 64 static pressure taps located on both suction and pressure sides, with one on the base. The CTE 1 and CTE 2 shapes comprise one and two supplementary pressure taps in their base, respectively.

2.3. Test conditions

The experiments are conducted for a tunnel water speed of 2 ms^{-1} ($\pm 1\%$) and a water temperature of 293 K (± 2 K). This leads to a free stream Reynolds number based on the model c of about 800 000.

Transition is tripped on the lower and upper sides of the model by a 0.2 mm diameter trip wire, stuck parallel to the leading edge, at about 3% of c downstream of the leading edge.

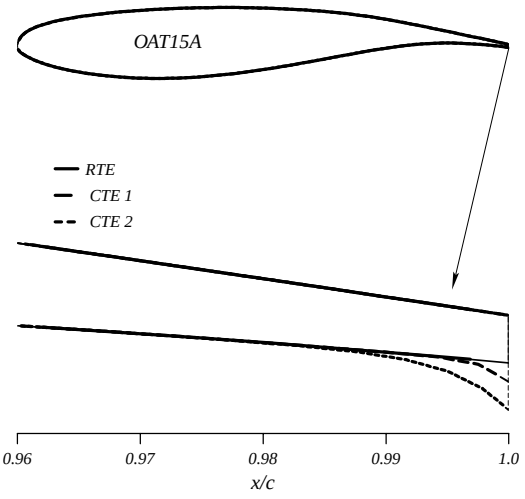

Fig. 1. Trailing edge definitions.

2.4. Measurements

A two-component LDV is used in a backward scattering mode; it allows to obtain the mean and fluctuating quantities of the velocity in a plane aligned with the upstream flow direction. Step-by-step motors under computer control do positioning of the measuring point in the X and Y directions.

Data acquisition is performed over about 2000 samples. Time needed for such an acquisition is used for calculating the mean value, the standard deviation and the correlation of the two velocity components for the point measured just before. According to the size of the measurement volume, no data could be obtained at a distance less than 0.2 mm to any model side or base.

Wake and boundary layer surveys have been performed in a single plane located at one-third of the span airfoil. Details about the measurement technique can be found in Pailhas et al. (1998) and Sauvage (1998).

3. Navier–Stokes solver and turbulence modelling

3.1. Governing equations

The "CANARI" code developed by ONERA, solves the three-dimensional compressible RANS system of equations (Vuillot et al., 1993, Couaillier, 1999). The perfect gas law is used to compute the static pressure. The diffusive fluxes of the RANS equations system are evaluated following the Stokes hypothesis and the Boussinesq assumption.

The molecular viscosity is given by the Sutherland law; the eddy viscosity being derived from the considered turbulence model. The viscous stress tensor and the heat flux vector are then related to the velocity gradient and temperature gradient, the standard and turbulent Prandtl numbers being assumed constant and equal to 0.72 and 0.9, respectively.

3.2. Turbulence modelling

Momentum and turbulence equations are decoupled; such a procedure should lead to the correct steady state. The code had originally an algebraic mixing length model (Michel et al., 1969) and a two-equation transport model (Jones and Launder, 1972) [JL]. Improvements were brought by Sauvage (1998) and Houdeville (1997) by extending the code with several one- and two-equation transport models, knowing that some of them have provided correct flow predictions for rather thick trailing edges (Stanaway and McCroskey, 1992, Ekatenaris and Menter, 1994, Monsen and Rudnik, 1995).

The following models have been selected for the present study:

The Baldwin and Barth (1991) [BB] and Spalart and Allmaras (1994) [SA] models which require the solution of a transport equation for a quantity, derived either from the turbulent Reynolds number R_t ([BB]) or from the eddy viscosity ([SA]).

The two-equation k–ε type models: [JL], Chien (1982) [Ch] and Nagano and Tagawa (1990) [NT]; these models differ essentially from (i) wall proximity treatment with damping functions expressed as a function of either y^+ or R_t; (ii) isotropic or non-isotropic dissipation rate ε.

The two-equation model k–l from Smith (1994) [Sm], derived from a k–kl model, uses an equation for the turbulent length scale, l. Near-wall treatment is eliminated, resulting in an equation which is easier to handle numerically.

The [BB] and k–ε type models require a specific treatment in the separated regions because of corrector-type functions of

either y^+ or R_t, while the [SA] and [Sm] models require only an appropriate estimate of the wall distance.

3.3. Numerical method

The solver is based upon a finite volume method; the discretization is cell-centred (grid points and flow variables are no longer collocated). In order to keep the modular feature of the solver, the time integration procedure requires an uncoupling of the RANS system and of the two-equation transport system. The former is solved with a frozen eddy viscosity; then, the latter is solved with fixed mean flow quantities. The algorithm involves a second-order accurate four stage Runge–Kutta scheme with an implicit residual smoothing; the local time stepping has been specified in order to satisfy a CFL stability criterion (Vuillot et al., 1993, Couaillier, 1999). Each fractional step can involve the succession of three stages: explicit calculation, artificial numerical dissipation correction and implicit resolution. Applying characteristic relations treats boundary and matching conditions.

3.4. Grid generation

This code admits multi-domain structured meshes with possible non-coincidence of the nodes or block overlapping.

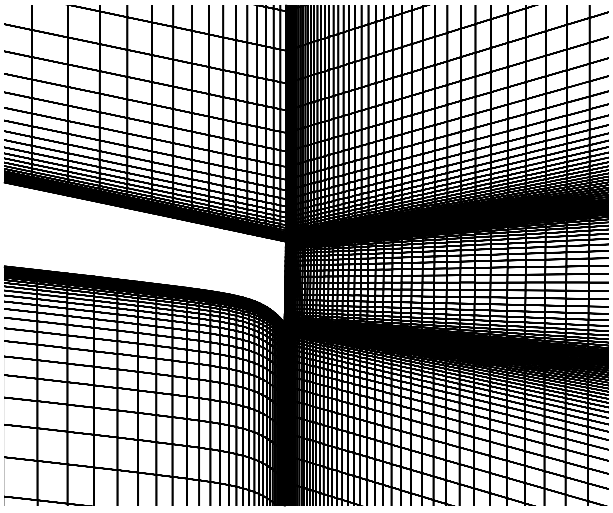

Fig. 2. Mesh refinement OAT15A-CTE 1 airfoil (zoom).

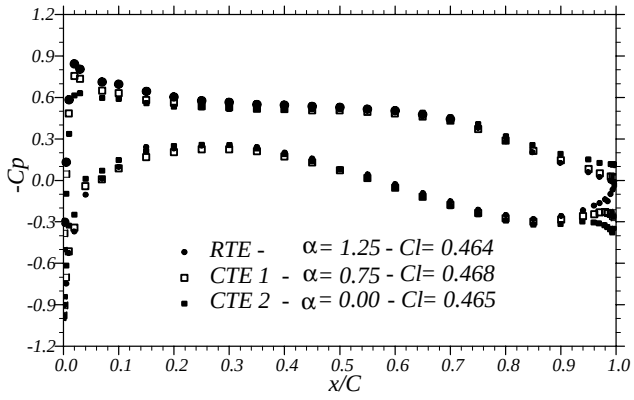

Fig. 3. Measured pressure distributions.

For our specific purpose, grid generation leads to a C–H mesh topology, satisfying the following requirements: outer boundaries as far as 10 c away from the airfoil (using the far-field vortex condition from Thomas and Salas, 1986) and a value of y^+ close to 0.3 in the trailing edge vicinity. Mesh convergence has also been verified (Sauvage, 1998).

Appropriate adaptation of the mesh refinement is necessary in each trailing edge vicinity. An example of mesh geometry is given in Fig. 2, for the OAT15A-CTE 1 airfoil with 216×100 ("C") and 130×247 ("H") mesh points, in the longitudinal $\times$ normal to the wall directions including 49 points in the base. The presence of any wind tunnel wall was not simulated ("infinite" atmosphere).

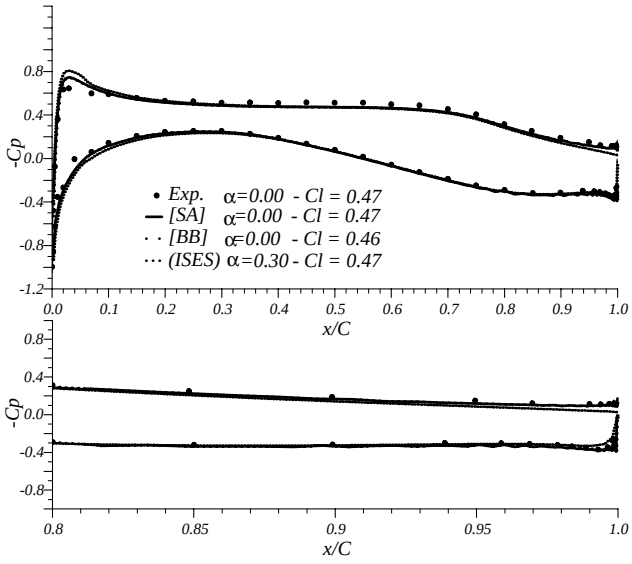

Fig. 4. Computed pressure distributions – OAT15A-CTE 2 airfoil (one-equation transport models).

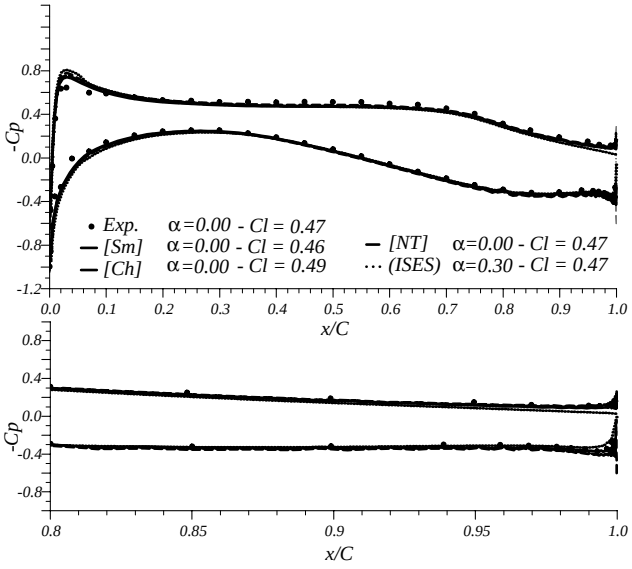

Fig. 5. Computed pressure distributions – OAT15A-CTE 2 airfoil (two-equation transport models).

4. Results and discussion

4.1. Pressure distribution along the airfoil

The measured longitudinal pressure distributions, obtained for the RTE, CTE 1 and CTE 2 trailing edges, are plotted in Fig. 3, for almost the same value of the lift coefficient (0.47).

The experimental Cp values have been corrected in order to take into account the wind tunnel "blockage" effect. In fact, the flow around the airfoil set in the hydrodynamic tunnel corresponds to the flow around the airfoil set in free stream conditions, but at a corrected velocity (Rogers, 1966) $(U_\infty)_c = U_\infty(1+\varepsilon)$, with $\varepsilon = (\pi/6)\cdot 0.77\cdot (c/h)^2 e_r$, where e_r is the thickness ratio, c the chord length of the model and h is the tunnel height.

As expected, an important pressure gradient modification is observed in the last 10% of c of both upper and lower sides of the airfoil. The combined effects of cambered lower side and increased divergence angle of the trailing edge result in an increase of rear airfoil loading, leading to smaller values of the angle of attack, for the same global lift coefficient. Indeed, $\Delta\alpha$ is equal to $-0.5°$ and $-1.25°$ for CTE 1 and CTE 2, respectively (cf. Fig. 3).

Computations with the above-mentioned turbulence models (cf. Section 3.2) are performed using the same grid. The value of the angle of attack used for such computations corresponds to the geometrical value corrected from wall effects, allowing to get approximately the right value of the lift coefficient (Pailhas et al., 1998, Sauvage, 1998). Whatever the turbulence model is, the agreement between experiments and computations is rather good, except maybe in the leading edge region where the correction due to the "blockage" might not be sufficient. An illustration is given in Figs. 4 and 5, for the thickest base OAT15A-CTE 2.

The pressure gradient variations in the rear part of the airfoil are very well reproduced by all models, including the decrease of the adverse pressure gradient on the upper side due to rear airfoil loading. On the last 5% of c of the lower side, the flow smoothly decelerates and then undergoes a very great acceleration due to camber. [Ch] and [NT] models are the only

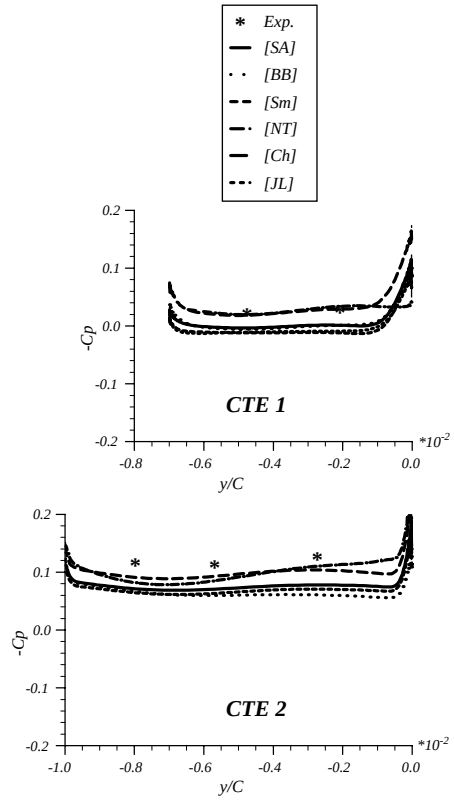

Fig. 6. Pressure distributions along the base of both OAT15A-CTE 1 and -CTE 2 trailing edges ($y/c = 0$ base/upper side, $y/c < 0$ base/lower side).

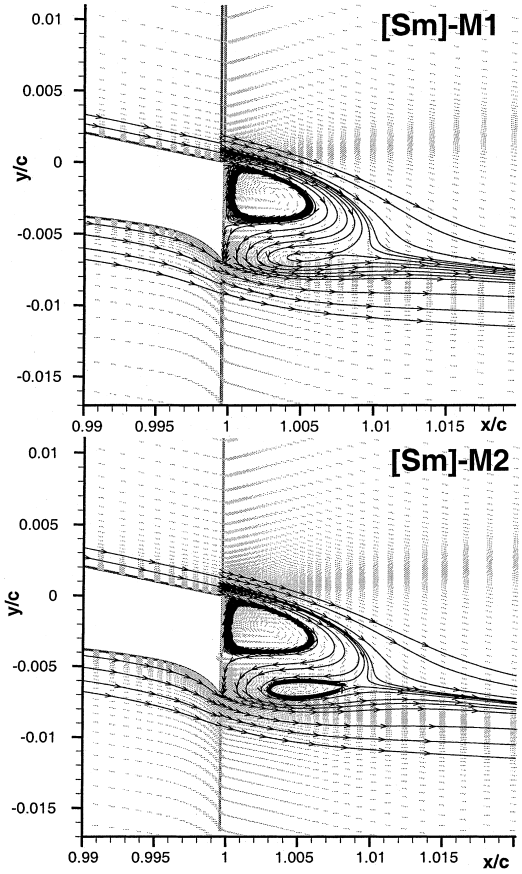

Fig. 7. Effect of grid refinement on topological structure (OAT15A-CTE 1).

Table 1
Estimations of base drag variations with cambered trailing edges

	$\Delta Cp_b = (-Cp_b)_{RTE} - (-Cp_b)_{CTE}$							
	Exp.	ISES	[BB]	[SA]	[Sm]	[Ch]	[JL]	[NT]
CTE 1	0.050	0.041	0.080	0.050	0.040	0.090	0.058	0.073
CTE 2	0.146	0.094	0.140	0.124	0.117	0.160	–[a]	0.141

[a] No convergence (cf. Section 4.3).

ones to slightly overpredict both the intensity of the adverse pressure gradient in that rear pressure side and the velocity peak in the leading edge vicinity. Modification of the overall circulation may explain it. Some oscillations appear on the last few percents of c along the lower side; they are attributed to mesh size distribution in this area with a rather strong camber.

It should be pointed out that the method used to define these trailing edge shapes (Drela and Giles, 1987) does not provide the correct pressure gradient behaviour in the rear part of the airfoil; indeed, it underestimates the increased rear loading. Such computations had been performed at a slightly higher value of the angle of attack than the Navier–Stokes ones.

4.2. Pressure distribution in the base

From experiments, the lower and upper surfaces appear to be uncoupled, since the pressure level on the upper side differs tremendously from that on the lower side. Therefore, the pressure coefficient along the base, Cp_b, is very close to the value recorded from the last pressure taps of the upper surface downstream of $x/C = 99\%$ (Sauvage, 1998). When looking at the computed Cp_b value, some differences exist depending upon the turbulence model (Fig. 6); anyhow, these computations allow to confirm the rather constant pressure level in the y-direction, hypothesised from 2 or 3 pressure taps, yet. Changes at the trailing edge between CTE 1 and CTE 2 are

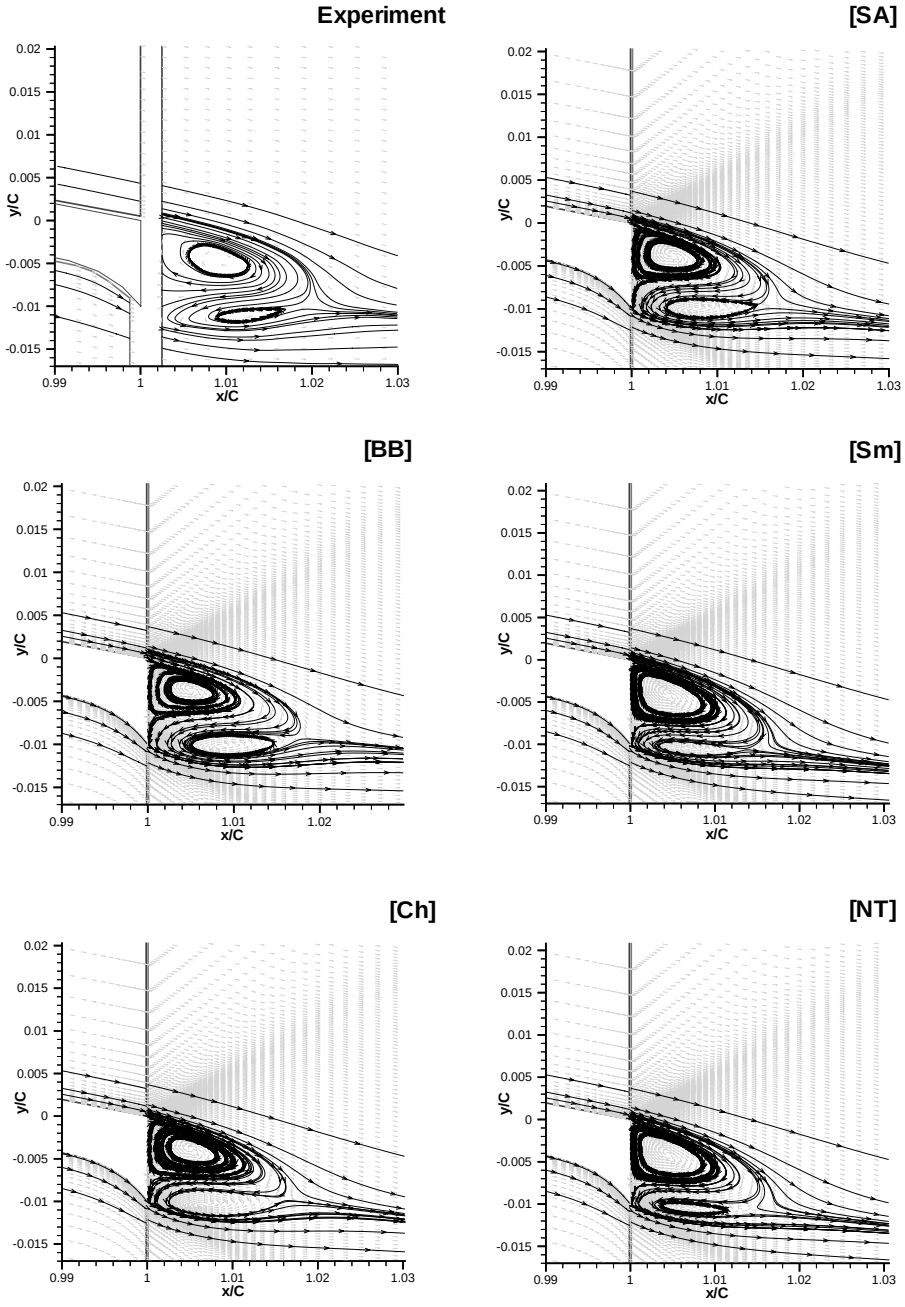

Fig. 8. Near-wake surveys downstream of the OAT15A-CTE 2 airfoil (zoom in the vicinity of the trailing edge).

directly related to the variation in the angle of attack, necessary for having a constant lift.

Integration along the base provides an average computed Cp_b value. Generally speaking, the models overestimate the pressure level along the base. The [Ch], [JL] and [NT] models predict a base pressure in better agreement with the experimental values than the [BB], [SA] and [Sm] ones. However, if one thinks of applying such a code for future optimisation, it is very important to guess correctly the base drag increase between the CTE 1 (or CTE 2) and the RTE, rather than the absolute value. [SA] and [Sm] provide the correct drag increase for the CTE 1 trailing edge; however, for the CTE 2 trailing edge, the [Ch] model overestimates the base pressure increase while the other models behave rather well. When comparing to the ISES estimates, improvements brought by using the CANARI code are noticeable (cf. Table 1).

4.3. Near-wake surveys

These experiments were mainly aimed at scrutinising the flow in the vicinity of the trailing edge. Downstream of the CTE 1 and CTE 2 bases, a recirculation area corresponding to negative longitudinal velocities is captured. When plotting the streamline pattern, two contra-rotating vortices are recorded in a confined area, the dimensions of which are tightly related to the base thickness (e): indeed, it is about $(2e \times e)$ in the longitudinal $\times$ transverse directions.

The computed topological structure is strongly dependent upon the mesh refinement downstream of the base. Illustration is provided in Fig. 7 for computations performed with the [Sm] model and two grids: M1 (and M2) "C"-type: 216×70 (216×100) "H"-type: 110×177 (130×247) with 39 and 49 grid points in the base, respectively. Indeed, the strength of the lower vortex can be more or less foreseen; such a refinement affects essentially the transverse component of the mean velocity and not the longitudinal one (Sauvage, 1998).

Computations of the viscous flow downstream of the OAT15A-CTE 2 airfoil are performed with different turbulence models, using the same refined mesh. For the thickest cambered trailing edge, couple of models revealed difficulty to reach convergence in the wake, especially on the transverse velocity component ρV. The reasons might be because of too much grid refinement in the transverse direction and/or existence of unsteady effects, which disappear slowly as long as iterations are pursued. Convergence was not possible with the [JL] model, yet; the shear stress profiles are very weak along the rear lower side of the cambered trailing edge. It looks as if the k–ε models hardly succeed to maintain turbulent flow in this area, amplifying then the apparent unsteady behaviour.

With the exception of the [JL] model, the other turbulence models allow to capture rather precisely these two vortex-type structures in the near-wake (Fig. 8). However, the computed vortices are located too close to the base, which is consistent with a too upstream location of the re-attachment point. Furthermore, the less extent of computed separated flow is in agreement with the computed weaker base-pressure values, compared to experimental values.

It could be pointed out that the camber of the lower side does not induce a "diving" motion of the flow. The suction effect due to the low base pressure counteracts the guiding of the flow by the strong variation of the geometry.

The level of the computed velocity modulus in the centre of the separation area is not in perfect agreement with the estimated one from wake surveys. Generally speaking, the turbulence models underestimate the maximum defect of the longitudinal velocity component in the wake, though its spreading along the longitudinal direction seems correct (Sauvage, 1998); illustration is given in Fig. 8 for several

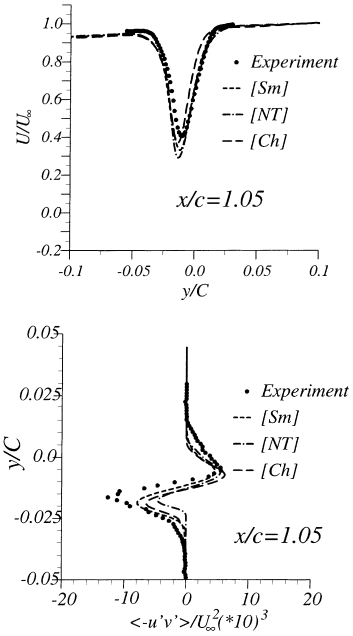

Fig. 9. U- and $u'v'$-profiles in the wake of the OAT15A-CTE 2 airfoil.

transport equation models. The plot of the shear stress profile in the near-wake reveals that no turbulence model is able to faithfully reproduce the recorded asymmetry between the upper and the lower parts of the wake (Fig. 9); the [BB] and [SA] models generate similar results to that given by the [Sm] one.

5. Discussions

Experiments carried out with an airfoil equipped with couple of increased cambered trailing edges have allowed to obtain a very precise description of the turbulent flow. The pressure gradient has been tremendously modified, especially in the last 10% of c on both sides of the airfoil, leading to an increase of the rear airfoil loading; the thicker the base, the larger the rear loading is. Thus, to reach a given lift coefficient, an airfoil with a cambered trailing edge has to be set at a lower angle of attack than that of the same airfoil with a "standard" base. Such a mechanism would allow to lessen wave drag for transonic conditions. However, this decrease of wave drag is related to an increase of the absolute value of the moment coefficient that should not be forgotten when dealing with aircraft optimisation.

A rather complete database, issued from boundary layer and wake surveys performed in each trailing edge vicinity, has been generated. A RANS solver, developed by ONERA, including several one- and two-equation transport turbulence models, has been applied to such aerodynamic configurations. All the tested models are able to reproduce rather correctly the physical and topological modifications induced by such cambered trailing edges, that were pointed out throughout the experiments.

Nevertheless, the Spalart–Allmaras and Smith models are producing results in better agreement with experiments than the other selected turbulence models; the former notably guess the consistent total drag increases, essentially due to base drag increase, eventhough not discussed in the present paper. The [SA] model is less sensitive to grid refinement than the [Sm] model, yet.

Applications of these models at transonic conditions will remain the following challenge, since it would lead to future optimisation of such trailing edge geometry for wing design.

The Spalart–Allmaras and Smith models have shown a great numerical robustness, which may be worth testing in RANS solvers devoted to compute possible complex industrial flow configurations.

Acknowledgements

The authors gratefully acknowledge the support that Airbus Industrie and the Service Technique des Programmes Aéronautiques have provided for the research reported in this paper.

References

Baldwin, B.S., Barth, T.J., 1991. A one-equation turbulence transport equation model for high Reynolds number wall-bounded flows. AIAA Paper 91-0610.

Chien, K.Y., 1982. Predictions of channel and boundary layer flows with a low-Reynolds number turbulence model. AIAA Journal 20 (1), 33–38.

Couaillier, V., 1999. Numerical simulation of separated turbulent flows based on the solution of RANS/low-Reynolds two-equation model. AIAA Paper 99-0154.

Drela, M., Giles, M.B., 1987. A two-dimensional viscous aerodynamic design and analysis code. AIAA Paper 87-0424.

Ekatenaris, J.A., Menter, F.R., 1994. Computation of separated and unsteady flows with one and two equation turbulence models. AIAA Paper 94-0190.

Henne, P.A., Greg III, R.D., 1991. A new airfoil design. J. Aircraft 28 (5), 333–345.

Houdeville, R., 1997. Formulation générale des modèles de turbulence à deux équations de transport dans CANARI. ONERA Technical Report 72/5025.61.

Jones, W.P., Launder, B.E., 1972. The prediction of laminarization with a two-equation model of turbulence. Int. J. of Heat and Mass Transfer 15 (2), 301–314.

Michel, R., Quemard, C., Durand, R., 1969. Application d'un schéma de longueur de mélange à l'étude des couches limites turbulentes d'équilibre. ONERA Technical Note 154.

Monsen, E., Rudnik, R., 1995. Investigation of the blunt trailing edge problem for supercritical airfoils. AIAA Paper 95-0089.

Nagano, Y., Tagawa, M., 1990. An improved k–ε model for boundary layer flows. Journal of Fluids Engineering, Transactions of the ASME 112, 33–39.

Pailhas, G., Sauvage, P., Touvet, Y., Coustols, E., 1998. Flow field in the vicinity of a thick cambered trailing edge. In: Proceedings of the Nineth International Symposium on Application of Laser Technology to Fluid Mechanics, Lisbonne, vol. 1:19-3-1;19-3-8.

Rogers, E.W.E., 1966. Blockage effects in closed or open tunnels. AGARDograph No. 109.

Sauvage, P., 1998. Étude expérimentale et numérique des écoulements potentiels et visqueux dans le voisinage d'un bord de fuite épais cambré. Ph.D Thesis SUPAERO Toulouse.

Smith, B.R., 1994. A near-wall model for the k–l two-equation turbulence model. AIAA Paper 94-2386.

Spalart, P.R., Allmaras, S.R., 1994. A one-equation turbulence model for aerodynamic flows. La Recherche Aérospatiale 1, 5–21.

Stanaway, S.K., McCroskey, W.J., 1992. Navier–Stokes analysis of blunt trailing edge airfoils. AIAA Paper 92-0024.

Thomas, J.L., Salas, M.D., 1986. Far-field boundary conditions for transonic lifting solutions to the Euler equations. AIAA Journal 24 (7), 1074–1080.

Vuillot, A.M., Couaillier, V., Lamis, N., 1993. 3D turbomachinery Euler and Navier–Stokes calculations with a multi-domain cell-centered approach. AIAA Paper 93-2576.